Transient Groundwater Flow Through a Coastal Confined Aquifer and Its Impact on Nearshore Submarine Slope Instability

N. Sultan, S. Garziglia, X. Bompais, P. Woerther, C. Witt, A. Kopf, Sébastien Migeon

JGR Earth Surface

RESEARCH ARTICLE
10.1029/2020JF005654

Transient Groundwater Flow Through a Coastal Confined Aquifer and Its Impact on Nearshore Submarine Slope Instability

N. Sultan[1], S. Garziglia[1], X. Bompais[2], P. Woerther[2], C. Witt[3], A. Kopf[3], and S. Migeon[4,5]

[1]Unité Géosciences Marines, Ifremer, Plouzané, France, [2]Unité Recherche et Développements Technologiques, Ifremer, Plouzané, France, [3]MARUM—Center for Marine Environmental Sciences, University of Bremen, Bremen, Germany, [4]Université Côte d'Azur, Observatoire de la Côte d'Azur, CNRS, IRD, Géoazur, Valbonne, France, [5]UFR939, Sorbonne Université, Paris, France

Key Points:
- A decade of pore pressure data reveals important groundwater exchange between a coastal aquifer and a nearshore submarine shelf
- Excess pore pressures are more likely the trigger of observed shear zones in a prone-to-failure area
- Earthquakes could accelerate the development of progressive slope failure by decreasing its factor of safety

Correspondence to:
N. Sultan,
nabil.sultan@ifremer.fr

Citation:
Sultan, N., Garziglia, S., Bompais, X., Woerther, P., Witt, C., Kopf, A., et al. (2020). Transient groundwater flow through a coastal confined aquifer and its impact on nearshore submarine slope instability. *Journal of Geophysical Research: Earth Surface*, *125*, e2020JF005654. https://doi.org/10.1029/2020JF005654

Received 13 APR 2020
Accepted 7 AUG 2020
Accepted article online 17 AUG 2020

Abstract Rare in situ pore pressure and temperature data sets collected over more than one decade in a submarine landslide-prone area off Nice (Southeast France) have been used to characterize a transient groundwater exchange between a coastal confined aquifer and the nearshore shallow-water submarine shelf. The near-coast study zone is highly exposed to geohazards and remains sadly famous for the 1979 catastrophic tsunamigenic submarine landslide with several casualties and substantial material damage. Measured pore pressure buildup does not appear to be synchronized with either the discharge of the nearby Var River or with precipitation in the Nice area. Unexpectedly, pore pressure fluctuations synchronizes well with seabed temperature trends indicating that the nearshore submarine shelf is mainly impacted by long smooth seasonal variations. We used the pore pressure and temperature data to describe the general transport mechanisms of pore waters and show that pore pressure diffusion is predominantly responsible for the near-seabed pore pressure buildup. Based on our results and previously published geotechnical data, slope stability calculations reveal that groundwater exchange has a major impact on slope instability and shear zone formation in a prone-to-failure area. Minor earthquake-induced ground accelerations seem to contribute to the nearshore slope instability by decreasing its factor of safety.

1. Introduction

The coastal areas around the Mediterranean Sea are exposed to major natural hazards, including earthquakes, landslides, volcanic eruptions, and tsunamis (de Lange et al., 2011). These hazards arise from the overall convergent tectonics of subduction, backarc spreading, and steep continental slopes fed by mountain-supplied rivers. Both historical and present-day catastrophic events are responsible for infrastructure destruction and numerous casualties. For the area surrounding the Nice study site, the most recent events causing massive damages are the 1887 Ligurian earthquake with its three successive earthquake shocks and its 2 m-high tsunami (Augliera et al., 1994; Christophe et al., 2012; Eva et al., 2001), and the 1979 submarine landslide (Habib, 1994). The study of the landslide geohazard in this area is particularly crucial since the Urban Community of Nice Area is one of the most significant economic centers in France, with over half a million permanent inhabitants and millions of tourists throughout the year (Pégaz-Blanc & Pérot, 2002).

The 1979 tsunamigenic submarine landslide is one of the rare submarine failures whose precise sequence of events was observed and partially described from the prefailure stage to the postfailure generation of a tsunami (Habib, 1994; Ioualalen et al., 2010; Mulder et al., 1997; Piper & Savoye, 1993). Since the 1979 event, the scientific community has acquired a large collection of geotechnical, geological, and geophysical data in the area showing that sectors of the shelf are still prone to failure. This is due to the presence of weak zones identified on piezocone soundings by Sultan et al. (2010). Kopf et al. (2016) acquired geotechnical and sedimentological data showing the presence of a shear zone in the 1979 landslide failure scar. Repeated bathymetric surveys acquired along the Nice continental shelf and upper slope from 1967 to 2011 were recently analyzed by Kelner et al. (2016) demonstrating that landslides with a volume of >25,000 m^3 can occur with frequencies of <8 years in the area of the 1979 event.

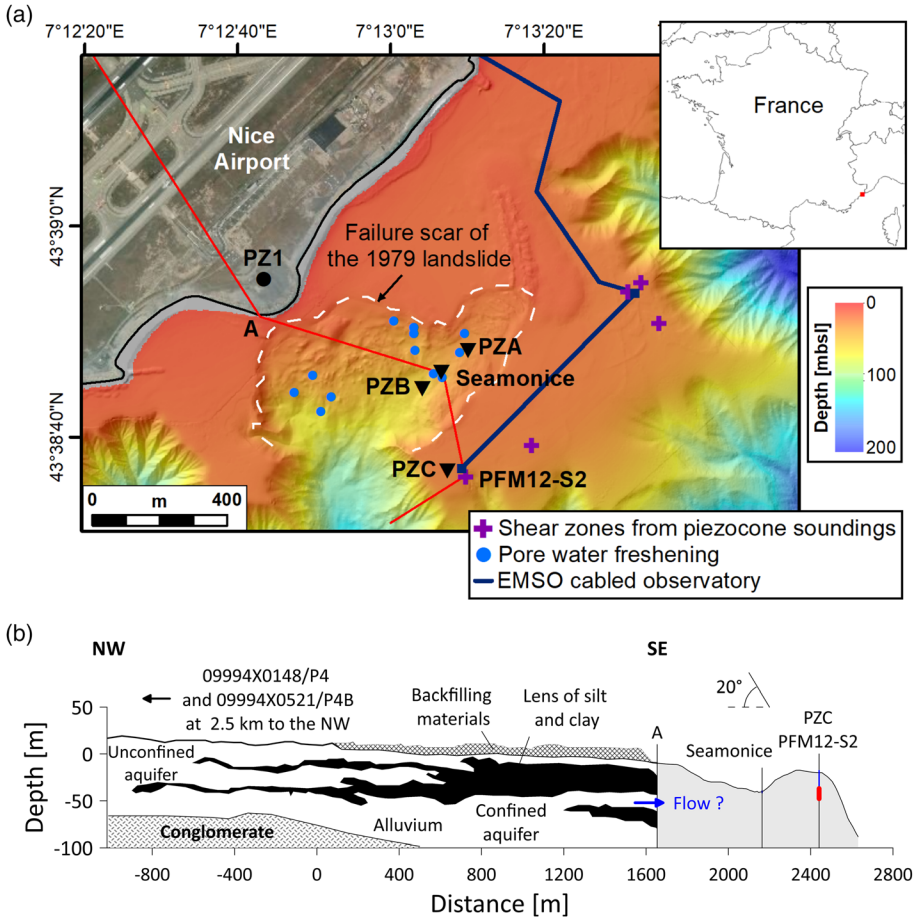

Figure 1. (a) Multibeam bathymetry data showing the locations of four offshore piezometer stations (Seamonice, PZA, PZB, and PZC), one onshore piezometer (PZ1) and one offshore piezocone site (PFM12-S2). Blue dots indicate pore water freshening described by Oehler et al. (2017). The red polyline indicates the location of the cross section shown in (b). (b) Composite geological profile through Var delta deposits (onshore and offshore) compiled from Emily et al. (2010) and Du et al. (2016). Red zone in (b) indicates the shear zone detected thanks to in situ piezocone data.

The continental shelf and slope off the Nice Airport (Figure 1) therefore represent a potentially unstable area where factors favoring instability were proposed to include (i) groundwater charging (Anthony & Julian, 1997; Kopf et al., 2010; Stegmann et al., 2011), (ii) weak sedimentary layers (Dan et al., 2007), (iii) high-sediment accumulation rates related to hyperpycnal flows (Dubar & Anthony, 1995; Mulder et al., 2001), (iv) highly liquefiable sediments (Roesner et al., 2019) in a geological context characterized by a strong amplification effect of seismic waves (Courboulex et al., 2020), (v) significant anthropogenic modification of the shores involving construction (Cavalie et al., 2015) and (vi) natural slope oversteepening (Kelner et al., 2016; Migeon et al., 2011).

The first long-term pore pressure data from the area were acquired thanks to the Seamonice piezometer that was deployed for a period of 1 year (November 2006 to November 2007) within the 1979 scar (location in Figure 1). Thanks to the data recovered, Stegmann et al. (2011) consider that elevated excess pore pressures, one of the main causal factors of landslides, were partially related to precipitation events and to the discharge flow of the Var River. Since this conclusion is supported by only a 1-year monitoring period, we believe that longer pore pressure and temperature time series are needed to conclude on the described link. In this work, in situ pore pressure data collected over more than one decade in the area will help provide an answer to the following question: Is there any link between coastal groundwater fluctuations and nearshore submarine slope instabilities?

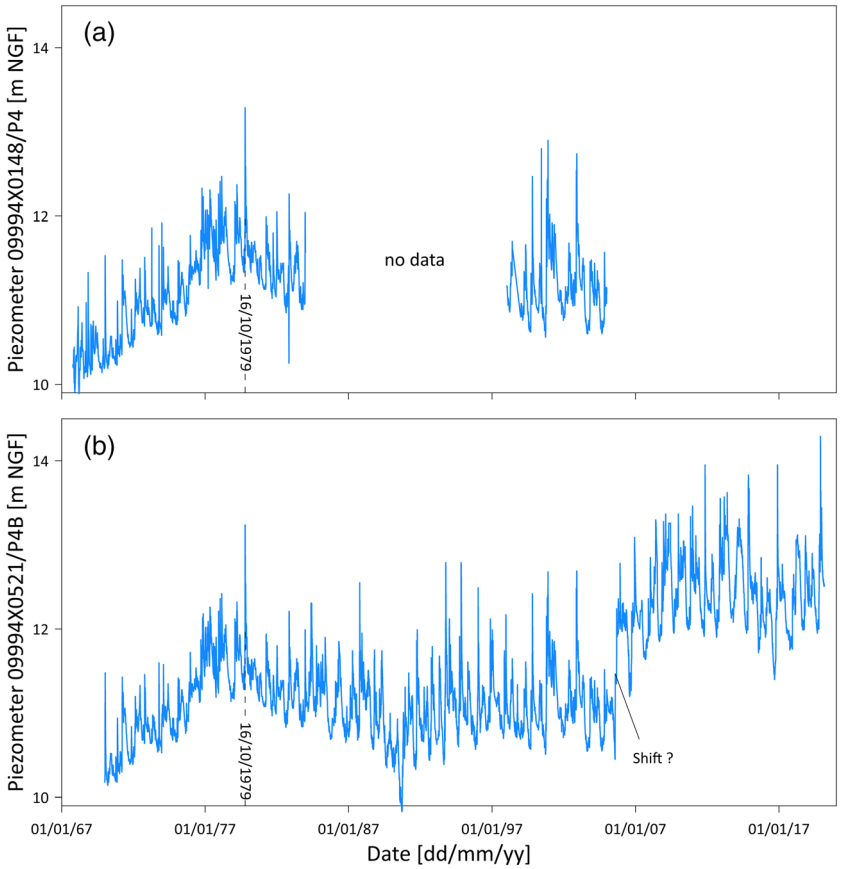

Figure 2. Groundwater level changes recorded over more than 45 years at around 5 km upstream from the 1979 failure scar (location and data on www.hubeau.eaufrance.fr). (a) Piezometer 09994X0148/P4 with the highest level (in m NGF = "Nivellement Général de la France") reached on 16 October 1979, corresponding to the date of the catastrophic Nice landslide. (b) Piezometer 09994X0521/P4B showing that during the period going from October 1970 to September 2005 the maximum NGF level was also reached on 16 October 1979.

The present paper deals with the correlation between groundwater fluctuation onshore and offshore monitored pore pressure and its implications in terms of submarine slope instability. This paper will thus provide new results better constraining one of the main factors potentially triggering shallow submarine landslides in a context of highly sedimented continental slopes connected with a coastal aquifer.

2. Geological and Hydrogeological Background

The Var submarine sedimentary system is located in the Ligurian Sea and extends off Nice and the Var and Paillon Rivers into the Western Mediterranean (Savoye et al., 1993). The Var delta front and the steep continental slope (locally exceeding 30°) are cut by major canyons and numerous smaller steep-sided valleys and gullies (Anthony & Julian, 1999; Klaucke & Cochonat, 1999; Migeon et al., 2012) with tens of landslides triggered at different locations along the delta front (Kelner et al., 2014). The lower Var-River valley (LVV) is characterized by the presence of three overlapping aquifers (Du et al., 2019): "the alluvium, the conglomerate, and the karstic limestone." Emily et al. (2010) used data from 56 drillings in the Var-River valley to derive a geological profile (Figure 1b) showing that the upstream part of the alluvial aquifer is unconfined while the presence of silt and clay lenses confines the alluvial aquifer near the mouth of the Var River (Figure 1). Du et al. (2016) confirmed the validity of the depositional geometry and sediment distribution affecting the unconfined aquifer by carrying out 3-D hydraulic modeling of groundwater flow in the LVV (Figure 1b).

Recently, Rohmer et al. (2020) showed that the sediment thickness is more than 100 m under Nice airport. The absence of drilling data in the offshore part of the Var delta prevents defining an accurate extension of

Table 1
Characteristics of Piezometers Used in the Present Study

#	EMSO names	Number of sensors	Coordinates	Water depth (m)	Length (m)	Recording period
PZA	ST5-PZ2L-02	5	N43.6467 E7.2192	27.0	4	30 April 2015 – 20 August 2019
PZB	GeoB-13,931	5	N43.6457 E7.2178	40.3	4.1	9 June 2009 – 3 September 2011
PZC	SPF-PZ3L-01	20	N43.6436 E7.21865	21.0	28.3	15 October 2015 – 21 June 2019

the silty and clayey lenses and therefore an accurate offshore extension of the confined aquifer. However, in situ piezocone geotechnical profiles acquired by Sultan et al. (2010) confirm the presence of low permeable silty-clay layers along the 28 m maximum penetration of the piezocone rods supporting the Guglielmi and Prieur (1997) description of the presence of a confined aquifer under impermeable sediments of the submarine Var delta.

By comparing data acquired from the deep confined aquifer between 1981 and 1984 (piezometer 10001X0801/PZ1 in Figure 1a—depth 101 mbsf) and the 09994X0148/P4 data (location in Figure 1b), Ciron et al. (1986) show that a good correlation and fast exchange exist between the alluvial unconfined and confined aquifers. Groundwater level fluctuations in the unconfined aquifer recorded over more than 45 years around 5 km upstream from the 1979 failure scar (09994X0148/P4 and 09994X0521/P4B piezometers—location and data on www.hubeau.eaufrance.fr), show that the highest measured piezometer level at 09994X0148/P4 was reached on 16 October 1979, the date of the Nice landslide (Figure 2a). For the 09994X0521/P4B piezometer, data recorded between October 1970 and September 2005 confirm that the maximum Nivellement Général de la France (NGF) level was also reached on 16 October 1979 (Figure 2b). By considering the Ciron et al. (1986) correlation between the two aquifers, it is possible to affirm that an exceptionally high piezometer level was reached in the nearshore confined aquifer on 16 October 1979 event. The question remains, however, as to how far the transmission of this exceptional excess pore pressure extended offshore and what role it played in generating the 1979 landslide (Dan et al., 2007; Stegmann et al., 2011).

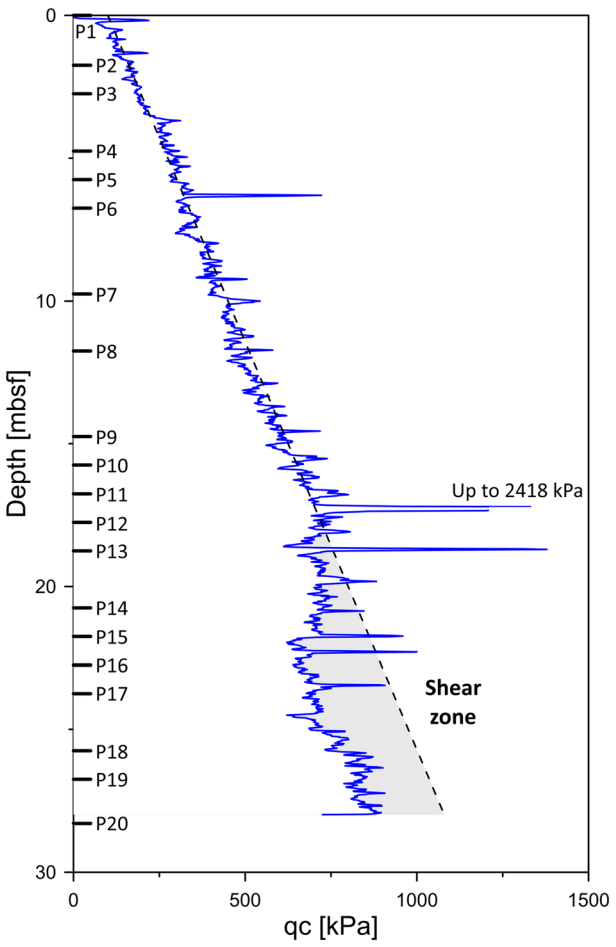

Figure 3. Sensor depths of the PZC piezometer shown together with the tip resistance (qc) obtained from site PFM12-S2 showing the presence of a well-formed shear zone (gray-shading) below 22 m below the seafloor (mbsf). Peak values of qc correspond to the presence of sandy/silty layers.

Pore pressure buildup decreases the effective stress and consequently weakens the slope sediment by decreasing its shear strength. By analyzing and describing several examples of onshore progressive failures (data from Bromhead, 1998, and Cooper et al., 1998), Leroueil (2001) illustrated how it is possible to bring the slope to failure by incrementally increasing pore pressure. In situ piezocone measurements carried out by Sultan et al. (2010) reveal the presence of several shear zones at the border of the shelf to the S-E of the 1979 landslide scar (Figure 1a), suggesting the initiation of a progressive failure mechanism. Increased pore pressure could be the cause of this shear zone formation since it may reduce the effective normal stress bringing the sediment to localized failure.

3. Materials and Methods

3.1. Onshore Piezometer Data and the Var River Discharge

According to Du et al. (2016), 24 piezometers are currently recording the piezometer groundwater level along the upstream part of the alluvial unconfined aquifer including piezometers 09994X0148/P4 and 09994X0521/P4B at around 5 km upstream from the 1979 failure

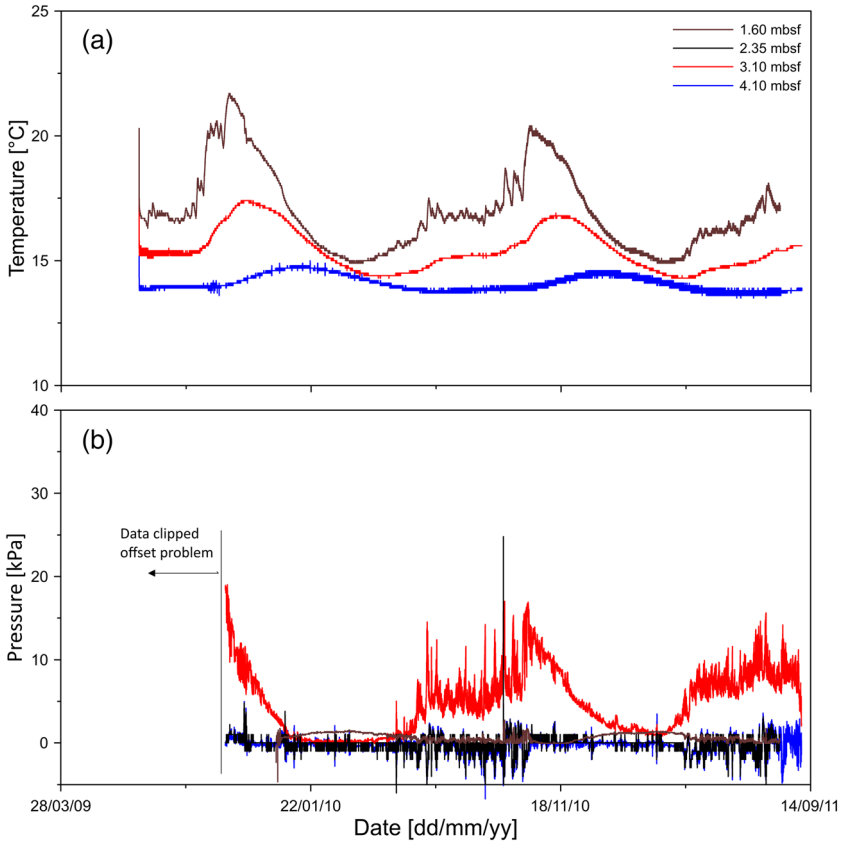

Figure 4. Data from PZB piezometer: (a) Temperature and (b) pore pressure versus time. Temperature sensor at 2.35 mbsf failed to record data. Temperatures recorded by the three sensors show an annual fluctuation trend while three of the four pore pressure sensors did not show significant pore pressure changes. Pore pressure sensor at 3.10 mbsf (red curve) shows a trend similar to that of temperature.

scar. These data, in addition to discharge data of the Var River (Pont Napoléon III, Nice) are available from this site (www.hubeau.eaufrance.fr).

3.2. Offshore Piezometers

In situ pore pressure measurements were carried out using cable-deployed piezometer equipped with a 60-mm diameter sediment lance with differential pore pressure and temperature sensors (Sultan & Lafuerza, 2013). Differential pore pressures were measured relative to hydrostatic pressure at different ports on the 60-mm diameter lance using specially adapted differential pressure transducers connected to the pressure ports and the open seawater. Piezometer pore pressure and temperature sensors have respectively an accuracy of $\pm$0.5 kPa and 0.05°C. The length of the lance measured between 3.95 and 4.10 m. Locations of the three piezometers (PZA, Seamonice and PZB) are shown in Figure 1.

A second type of piezometer (V3-type - Bompais et al., 2019) was developed to achieve deeper penetration by using the 50-kN capacity and the coiled tubing technique of the Penfeld penetrometer (Meunier et al., 2004) to push a 36-mm-diameter rod equipped with 20 differential pore pressure and temperature sensors.

In the framework of the EMSO seafloor observatory offshore Nice (Bompais et al., 2019), it was possible to acquire continuous real-time data from 15 October 2015 to 21 June 2019 with PZC (Garziglia et al., 2018). In addition, the stand-alone piezometer PZA recorded data from 30 April 2015 to 20 August 2019 with yearly diver operations to change the battery. While the PZA piezometer was deployed in the 1979 scar, PZC was deployed in an area considered as prone to failure after the detection of a shear zone from the piezocone sounding PFM12-S2 (Figure 1 and Table 1). The depth of the 20 sensors of PZC are projected in Figure 3

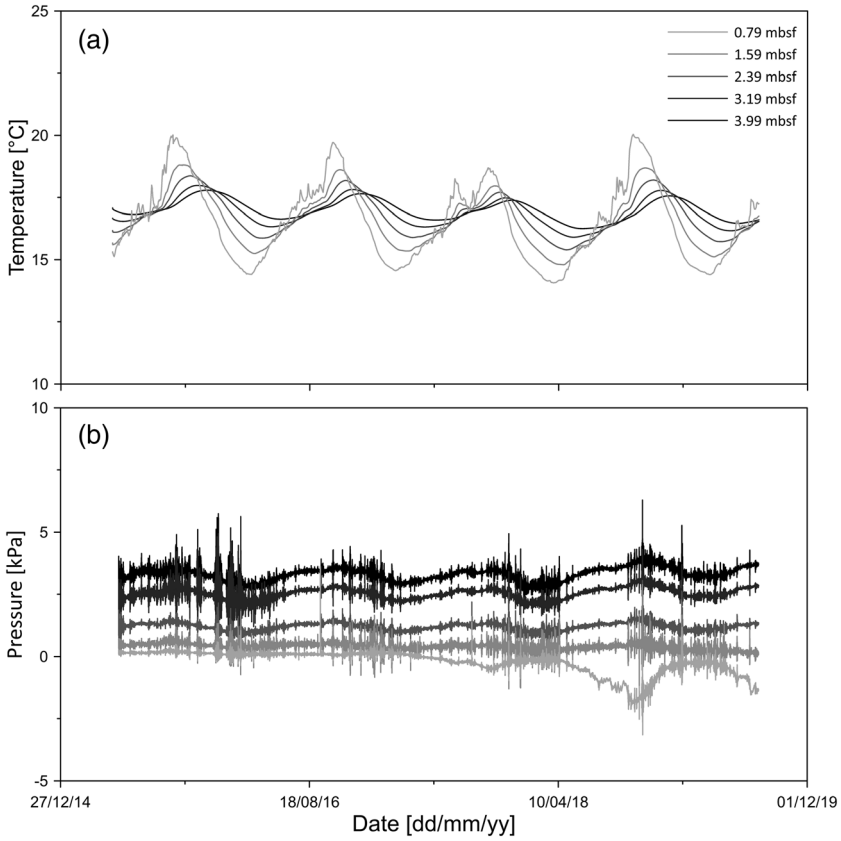

Figure 5. Data from PZA V2-type piezometer: (a) temperature and (b) pore pressure versus time. Temperatures and pressure recorded by the five sensors show a strong annual fluctuation.

together with the tip resistance (qc) obtained from site PFM12-S2 showing the presence of a well-developed shear zone below 22 m below the seafloor (mbsf). The distance between PZC and PFM12-S2 is around 60 m (locations are shown in Figure 1 and Table 1).

3.3. Modeling of Unsteady Thermal and Hydraulic Diffusion Processes

To understand the factors affecting the temperature and pressure field fluctuations measured by offshore piezometers, a 1-D unsteady thermal diffusion Equation 1 and hydraulic diffusion Equation 2 were solved numerically using a centered explicit finite difference discretization scheme.

$$\frac{\partial T}{\partial t} = \frac{\partial}{\partial z}\left(k_T \frac{\partial T}{\partial z}\right) \tag{1}$$

$$\frac{\partial u}{\partial t} = \frac{\partial}{\partial z}\left(k_u \frac{\partial u}{\partial z}\right) \tag{2}$$

In Equations 1 and 2, k_T and k_u signify, respectively, the thermal and hydraulic diffusivities of the material, T the temperature field, u the pore pressure field, t is the time ($t \geq 0$) and z ($0 \leq z \leq L$) is the space variable. The solution to Equations 1 and 2 requires specification of boundary conditions at $z = 0$ and $z = L$ and initial conditions at $t = 0$.

3.4. Infinite Slope Stability: Pseudo-Static Analysis

Pseudo-static analysis in seismic slope stability analysis considers that failure occurs when the shear stress on a surface parallel to the slope exceeds the shear strength of the sediment. The factor of safety (FoS) for

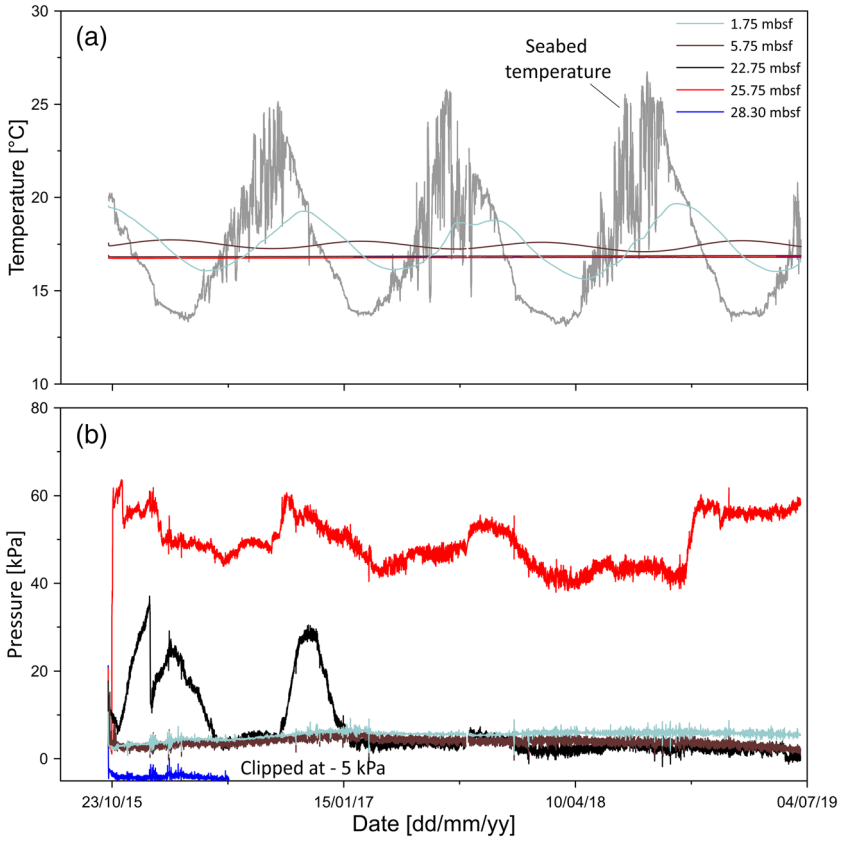

Figure 6. Data from five selected sensors of the PZC V3-type piezometer: (a) temperature and (b) pore pressure versus time. Seafloor temperature (light gray curve in a) and the upper four temperature sensors (P2 to P5) show strong annual fluctuations while the deepest temperature sensors (below P6 at 6.75 mbsf) show constant temperatures during the monitoring period. Pore pressure sensors P16 and P18 recorded significant pressure fluctuations.

infinite slope under drained conditions and zero cohesion is calculated according to (Hadj-Hamou & Kavazanjian, 1985) Equation 3:

$$FoS = \frac{\text{Shear strength}}{\text{Shear stress}} = \frac{[\sigma'_v \cos^2(\alpha) - \Delta u] \tan(\varphi')}{\sigma'_v \cos(\alpha) \sin(\alpha) + K_h \sigma_v \cos^2(\alpha)} \quad (3)$$

In Equation 3, σ_v and σ'_v are respectively the total and in situ effective vertical overburden stress, Δu is the excess pore pressure, φ' is the internal friction angle, α is the slope angle, and K_h is the horizontal acceleration in g's ($g = 9.81$ m/s^2). Slope failure will occur whenever the FoS falls below one.

4. Results

4.1. Pore Pressure and Temperature Data

The PZB piezometer was deployed in the 1979 scar at a water depth of 40.3 m (Figure 1 and Table 1). It acquired pore pressure and temperature data for more than 2 years (from 9 June 2009 to 3 September 2011). Data from the PZB piezometer are shown in Figure 4. Four pressure and three temperature sensors recorded the temperature and pressure conditions between 1.6 mbsf (brown curve) and 4.10 mbsf (blue curve, Figure 4). Temperatures recorded by the three sensors show annual fluctuations (between 13.7°C and 21.7°C); while three of the four pore pressure sensors did not record any significant pore pressure changes. The pore pressure recorded at 3.10 mbsf (red curve, Figure 4) shows a trend similar to that of temperature with values fluctuating between 0 and 19 kPa.

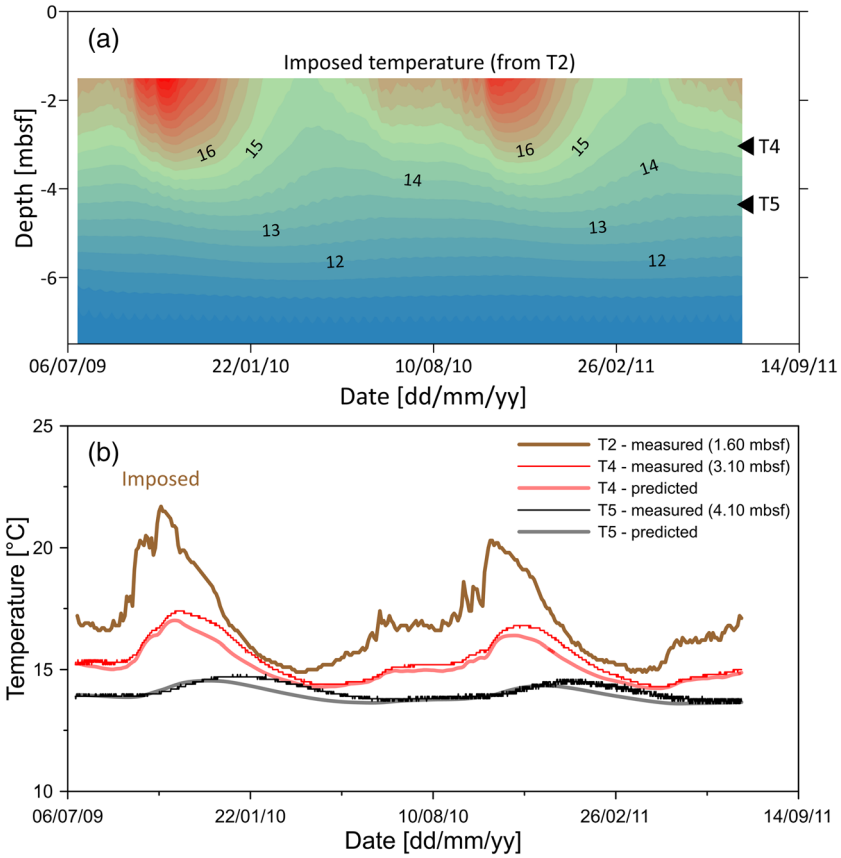

Figure 7. PZB site: (a) Calculated temperature field and its development during the 2-year monitoring period with imposed temperature at the level of the sensor T2 (at 1.6 mbsf). The calculated temperature field is obtained by solving the 1-D heat Equation 1. (b) Comparison of measured and predicted temperature versus time at levels 3.10 and 4.10 mbsf.

The piezometer PZA was installed at a water depth of 27 m (location in Figure 1) during a period exceeding 4 years. This piezometer was equipped with five sensors installed between 0.79 and 3.99 mbsf (Figure 5). Temperature and pressure recorded by the five sensors reveal marked annual fluctuations. While temperature fluctuations show an increasing delay with depth, pore pressure fluctuations at different depths remain in phase. Temperature sensors recorded values between 14°C and 20°C while pore pressure fluctuates between −1 and +6 kPa.

The PZC installed in the prone-to-failure area at a water depth of 21 m (location in Figure 1) acquired data during a 4-year period (from 15 October 2015 to 21 June 2019). PZC was equipped with 20 temperature and pressure sensors distributed between 0 and 28.3 mbsf (Figure 3). Data from five selected sensors of this V3-type piezometer are shown in Figure 6. Seafloor temperature (light gray curve in Figure 6a) and the upper four temperature sensors (P2 to P5) show strong annual fluctuations while sensors located deeper than 6.75 m below the seabed recorded constant temperatures during the monitoring period. Pore pressure sensors P16 and P18 recorded the most significant pressure fluctuations (maximum pore pressure 64 kPa at P18). Pore pressure at P18 fluctuated throughout the monitoring period while at P16 it became almost stable from 28 January 2017. Some of the shallow sensors (not shown in Figure 6) recorded pore pressure fluctuations which were correlated with tide fluctuations and the presence of free gas partially saturating the shallow sediments (Garziglia et al., 2019).

4.2. Thermal Regimes

Temperature changes measured at sites PZA, PZB, and PZC could be the result of (i) diffusion of seasonal seafloor temperatures and (ii) water advection through highly permeable sediment (fractures

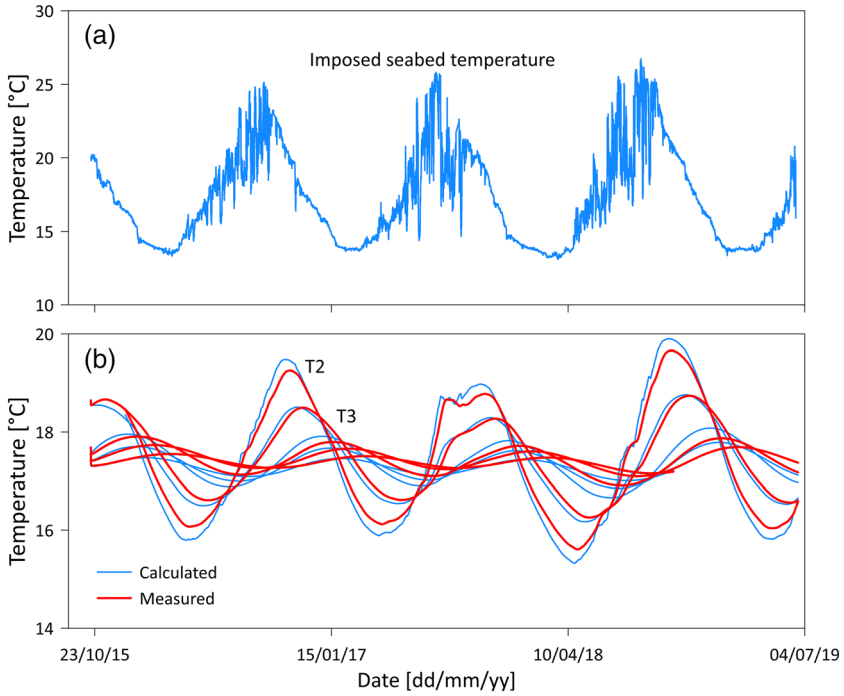

Figure 8. PZC: (a) Temperature fluctuations imposed at the seabed level. (b) Comparison of measured (red curves) and predicted (blue curves) temperature versus time for the succeeding five different sensors (at 1.75, 2.75, 4.75, 5.75, and 6.75 mbsf).

and sandy/silty layers). To identify the main thermal processes affecting temperature fields at the monitored sites, we considered as a working hypothesis that seafloor temperature diffusion is the main source of the measured temperature fluctuations. To calculate the effect of these seafloor temperature changes at the level of the different temperature sensors deeper in sediment, we used the heat Equation 1.

For the piezometer PZB, temperature imposed on the upper boundary was taken as equal to the temperature measured at sensor 2 (at 1.6 mbsf) and the initial temperature-depth profile was taken as equal to the mean temperature measured at the considered site. The thermal diffusivity values were taken equal 10^{-7} m^2/s above 3.5 mbsf and 10^{-6} m^2/s below this depth. These values were defined by a trial and error method. Figure 7a shows the calculated temperature field and its development during the 2-year monitoring period. The comparison of measured and predicted temperature versus time at levels 3.10 and 4.10 mbsf is shown in Figure 7b.

For the piezometer PZC, $T(0, t)$ was taken as equal to the seabed temperature (Figure 8a) and the initial temperature-depth profile was taken as equal to the mean temperature measured at the considered site. As for PZB, the thermal diffusivity values were considered varying between 10^{-6} and 10^{-7} m^2/s. Comparison of measured and predicted temperature versus time for the succeeding five different sensors (at 1.75, 2.75, 4.75, 5.75, and 6.75 mbsf) is shown in Figure 8b.

4.3. Hydraulic Regimes

Synchronous pore pressure perturbations were measured over almost 30 months by PZA and PZC/P18 (Figures 5 and 6). The pore pressure cycle recorded over a 1-year period by both piezometers fits well with the seabed temperature. Synchronous pore pressure variation for PZC was localized at only one level (P18) and partially at level P16 while the PZA recorded pore pressure fluctuations along the three deeper sensors. Our working hypothesis is that a common source feeds, through a permeable medium, sedimentary layers equivalent in depth to PZC/P18. However, at PZA site, the presence of highly permeable sediments allows the vertical diffusion of pore pressure. To check the validity of this hypothesis, a one-dimensional transient fluid flow model is used (Equation 2). For the present case, the pore pressure imposed at the

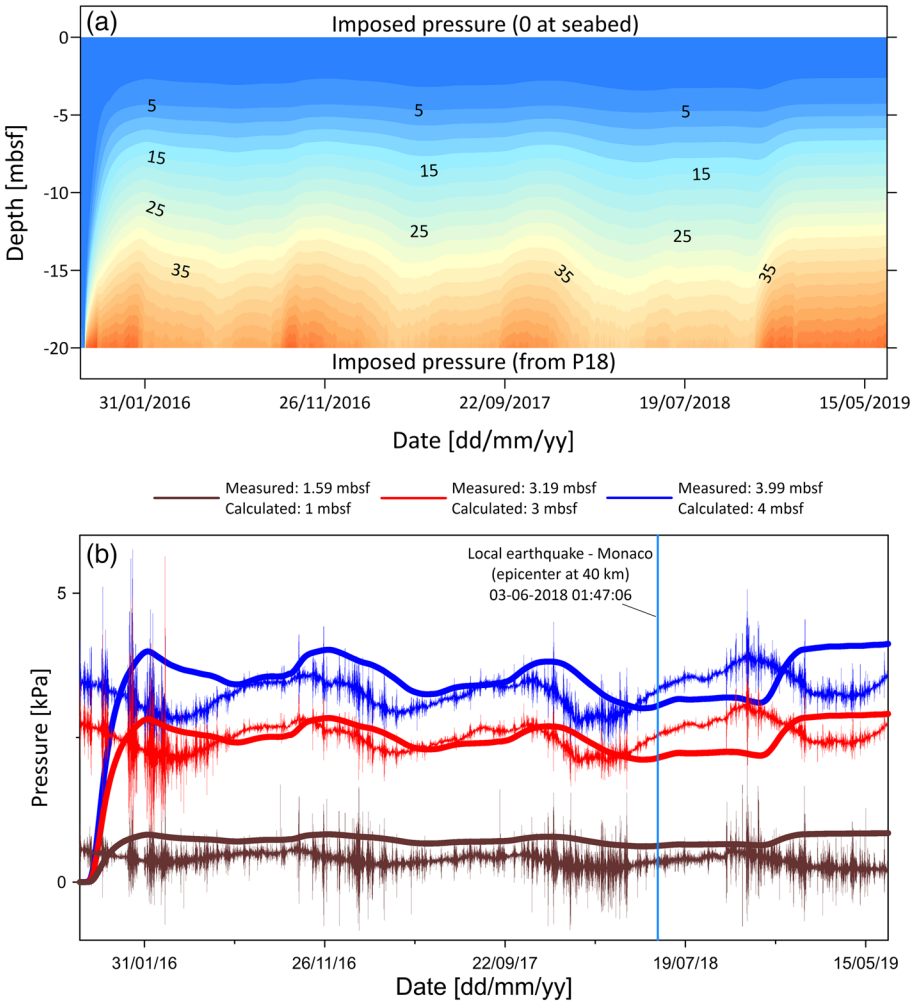

Figure 9. PZA site: (a) Calculated pressure field and its development during the 3-year monitoring period with an imposed pressure at 20 mbsf (P18 from PZC). The calculated pressure field is obtained by solving the 1-D hydraulic diffusion Equation 2. Numerical values indicate the pore pressure in kPa. (b) Comparison of measured (noisy curves) and predicted (continuous curves) pressure versus time at three different levels.

base of the model $u(L, t)$ is equal to the pressure measured at P18. L was calculated from the water depths at PZA and PZC and from the depth below the seafloor of the sensor PZC/P18 ($L = 21 + 25.75–27 \simeq 20$ m). The pore pressure imposed at the seabed $u(0, t)$ was taken as equal to zero (hydrostatic conditions). Hydraulic diffusivities ranging linearly from 5 10^{-5} m^2/s at $L = 0$ m to 1.3 10^{-5} m^2/s at $L = 20$ m. These were defined by a trial and error method. Figure 9a shows the iso-contour map of the calculated pore pressure u at site PZA. Comparison of measured (noisy curves) and predicted (continuous curves) pressure versus time at three different levels are shown in Figure 9b.

5. Discussion

The analysis of in situ pore pressure and temperature data collected over more than one decade in the area of the so-called 1979 failure offshore Nice leads us to discuss the following three main questions:

5.1. What Are the Main Factors Affecting the Measured Temperature Changes?

Figure 7a shows that the imposed temperature fluctuations diffuse slowly through the sedimentary column at site PZB. It is clear that during the 2-year calculation period, only the 3-m depth below sensor T2 is affected by temperature fluctuations (Figure 7a). The good agreement between measured and predicted

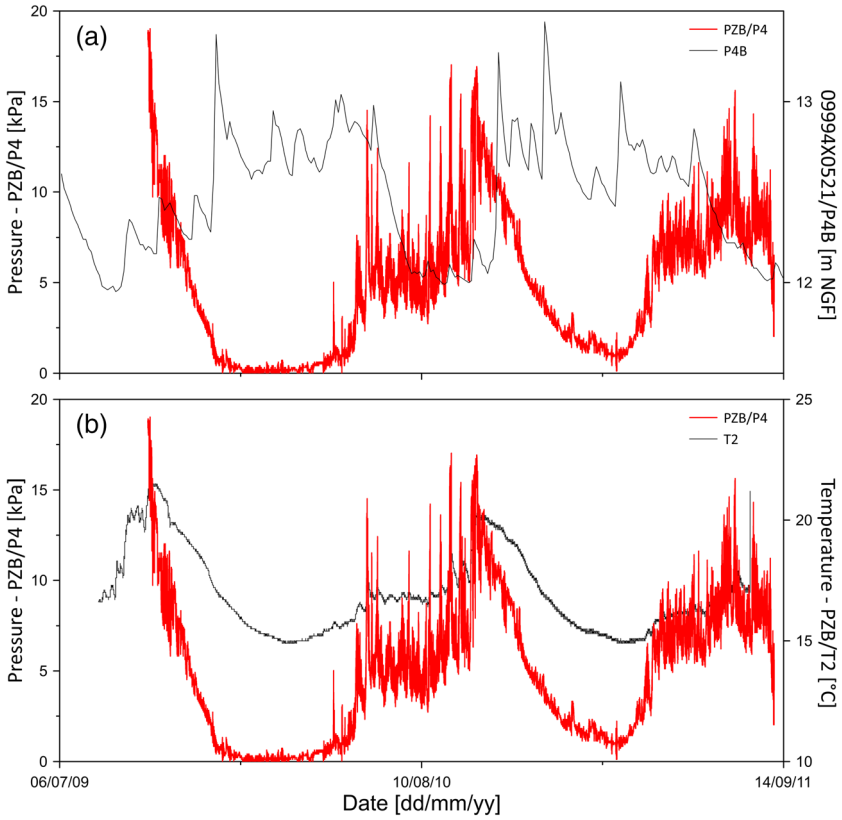

Figure 10. PZB/P4 pore pressure data (depth 3.10 mbsf) compared to (a) groundwater level changes recorded at 09994X0521/P4B located at around 5 km upstream of PZB and (b) the temperature measured by sensor T2 (1.6 mbsf) of PZB.

temperature versus time at levels 3.10 and 4.10 mbsf confirms the initial hypothesis concerning vertical diffusion as a major process controlling the temperature field in the upper sedimentary layers at PZB site (Figure 7b). Temperature calculations carried out at PZC (Figure 8) and at PZA confirmed the general impact of seabed temperature fluctuations on the temperature field in the sediments and established that vertical thermal diffusion is the main process controlling the temperature fluctuations at the three studied sites.

5.2. Is There Any Link Between Measured Pore Pressure Variability and External Forcing?

While diffusion was shown to be the main process controlling temperature fluctuations for the three piezometers (PZA, PZB, and PZC), it is clear that the cause of the pore pressure oscillations shown in Figure 4 (PZB) and Figure 6 (PZC) is not related to upward advection or diffusion of water. PZB piezometer data indicate that pore pressure fluctuated significantly only at the P4 intermediate sensor and only the P16 and P18 sensors of piezometer PZC recorded significant pore pressure fluctuations. On the other hand, PZA pressure data indicate synchronous seasonal fluctuations for all pressure sensors (Figure 5) showing that vertical pore pressure diffusion is possible at this location. Figure 1 suggests that the pore pressure fluctuations may be related to the groundwater level of the coastal confined aquifer and that lateral advection (PZB and PZC) and vertical diffusion (PZA) through thin sandy/silty layers, similar to those identified in Figure 3, are responsible for the observed pore pressure changes. Ciron et al. (1986) show that this coastal confined aquifer is directly impacted by the Var river discharge. Unfortunately, the lack of groundwater level data from the confined aquifer during the monitoring period precludes identifying a transfer function for the exchange between the confined aquifer and the observed shear zone.

Figure 10a shows PZB/P4 pore pressure data (depth 3.10 mbsf) compared to groundwater level changes recorded at 09994X0521/P4B site. It is important to note that 09994X0521/P4B provides the groundwater

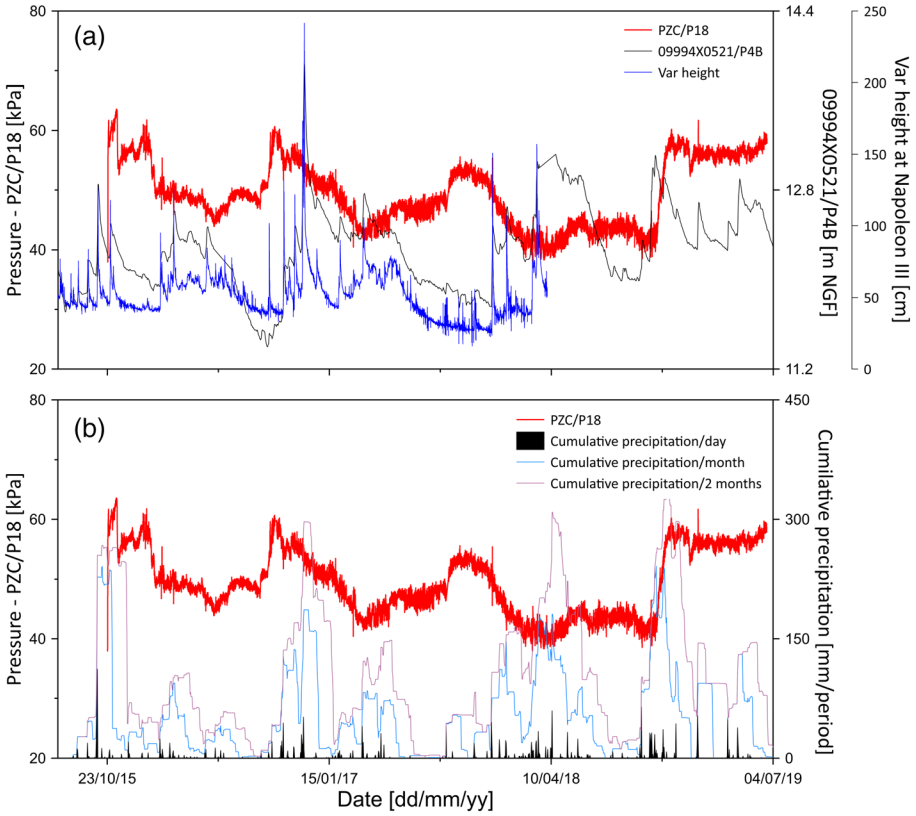

Figure 11. PZC/P18 pore pressure data (depth 25.75 mbsf) compared to (a) groundwater level changes recorded at 09994X0521/P4B and the Var height water level recorded at Napoleon III station and (b) the cumulative precipitation during 1 day, 1 month, and 2 months in the Nice region.

level of the unconfined aquifer. The comparison in Figure 10a demonstrates that pore pressures in the 1979 scar are not directly impacted by fluctuations measured in the unconfined aquifer. A delay of several months, exceeding the few-week period identified by Stegmann et al. (2011) exists between the two curves (Figure 10a). However, Figure 10b shows strong correlation between PZB/P4 pore pressure data and the near seabed temperature measured by sensor PZB/T2.

Figure 11a shows the PZC/P18 pore pressure data compared to groundwater level changes recorded at 09994X0521/P4B site and to the Var water level recorded at Napoleon III station. Figure 11a confirms previously described data (Du, 2016) concerning the excellent correlation between the unconfined aquifer and Var River discharge. On the other hand, and as shown for PZB, pore pressures at the level of the 1979 scar are not directly impacted by the groundwater head measured in the unconfined aquifer. Figure 11b highlights the absence of any correlation between cumulative precipitation over 1 day, 1 month, and 2 months in the Nice region and PZC/P18 pore pressure data. From Figures 10 and 11, it is plausible to conclude that the pore pressure fluctuations monitored in the scar of the 1979 landslide and at an equivalent level in the shear zone farther south bear no direct time relationship to the discharge of the nearby Var River nor to precipitation in the Nice area.

Assuming that the artesian flow through the confined aquifer contributed to the 1979 landslide (Figure 2), one would expect fast exchange between the Var River, the confined aquifer, and the base of the 1979 slide during exceptional flooding periods. However, our data show that this supposed exchange did not occur during the one decade monitoring period (Figures 10 and 11) They rather support a slow groundwater flow which can be reconciled with evidences reported by Garnier and Gounon (1984) indicating the presence of an impermeable limit along the shore partially isolating the confined aquifer from the offshore sediment deposits. The absence of temperature fluctuations measured by PZC deep sensors (P16, P18, and P20 in Figure 6a) confirms the presence of a slow water flow preventing lateral heat transfer.

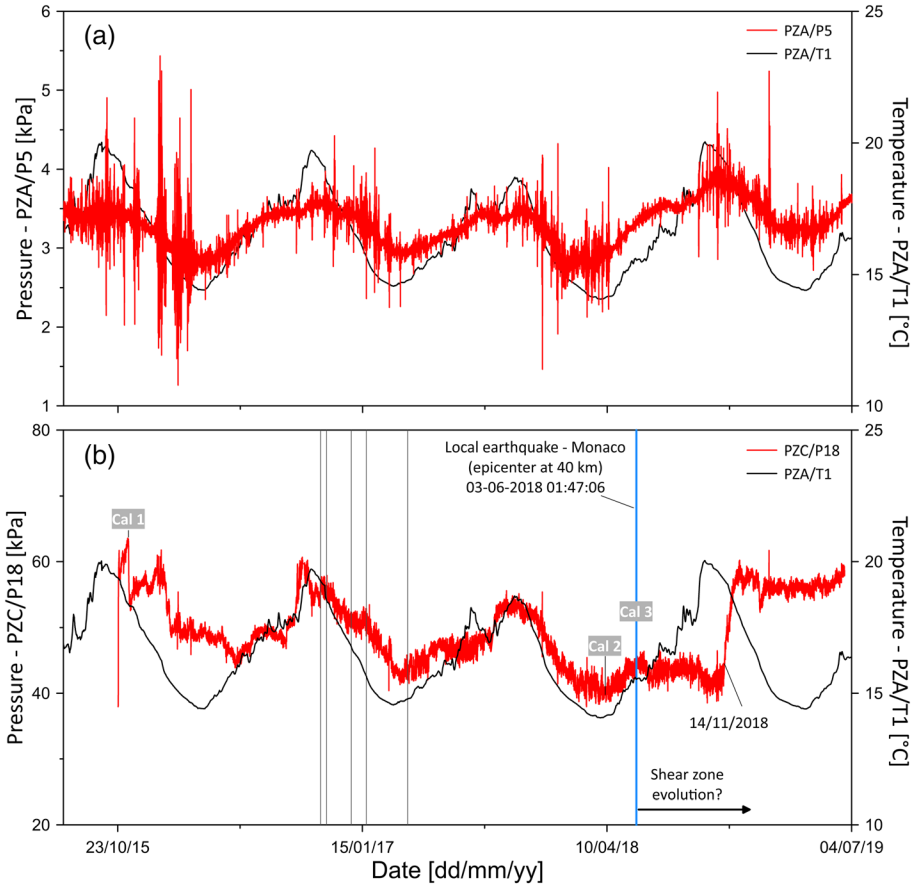

Figure 12. (a) ST5-PZ2L-02PZA/P5 and (b) PZC/P18 pore pressure data (depth 3.99 mbsf) compared to temperature measured by sensor PZA/T1 (0.79 mbsf) of ST5-PZ2L-02 and (b) SPF-PZ3L-01/P18 pore pressure data (depth 25.75 mbsf) compared to seabed temperature at SPF-PZ3L-01. Six earthquakes recorded by a broadband seismological station (PRIMA) installed offshore Nice airport (Courboulex et al., 2020) are shown in (b) as vertical lines (from left to right: Norcia-Central Italy, Digne-South of France, Chile, Solomon, Limone-northern Italy, and Monaco-offshore). Blue line in (b) indicates the local earthquake that occurred in offshore Monaco, 40 km from the study site (Courboulex et al., 2020) is indicated on both figures.

Comparing PZA/P5 (depth 3.99 mbsf) and PZC/P18 (depth 25.75 mbsf) pore pressure data with PZA/T1 (0.79 mbsf), shows that pore pressure data fluctuations fit well with seabed temperature changes (until 3 June 2018 for PZC - Figure 12b). The PZC/P16 pore pressure also fluctuated synchronously with seabed temperature during the first 2-year period of monitoring but became almost stable from 28 January 2017. Periods of strong correlation between seabed temperature and monitored pore pressure indicate that the measured pore pressure is impacted mainly by long smooth seasonal changes and that the low permeability of silt and clay offshore deposits modulated changes in groundwater head measured in the unconfined aquifer.

The change in synchronicity of PZC/P16 (after 28 January 2017) and PZC/P18 (after 3 June 2018) could be the result of fluid flow processes (ground water level, fluid circulation) or localized shearing processes and shear zone activation. Figure 12b shows six earthquakes recorded by a broadband seismological station (PRIMA) connected to the EMSO observatory near piezometer PZC (Courboulex et al., 2020). The ground accelerations recorded at PRIMA indicate a large amplification of the seismic waves but the maximum peak ground accelerations did not exceed 0.001 g, where *g* is the acceleration of gravity. There is no clear correlation between the first five remote earthquakes and the PZC/P16 and PZC/P18 pore pressure signals. However, an important aspect to comment on is related to the local *M*3.1 earthquake which occurred on 3 June 2018 in the area of the city of Monaco, 40 km away from the study site (vertical blue line in Figure 12b). After this event, the pore pressure changes recorded by PZC/P18 no more followed seabed

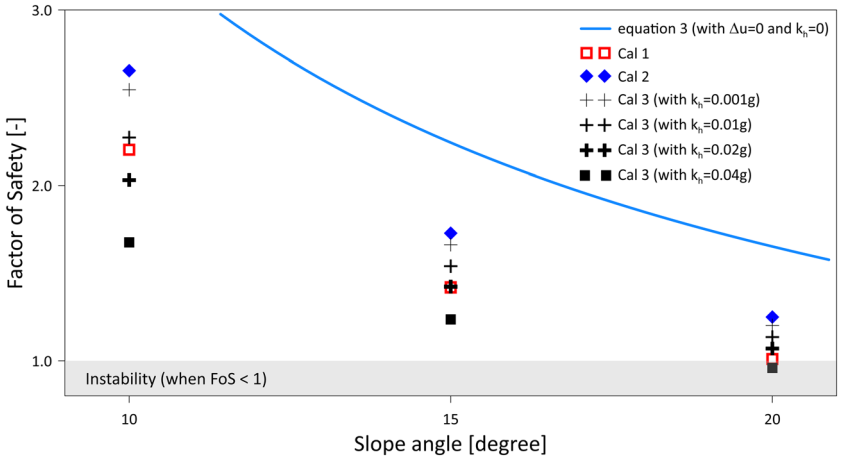

Figure 13. Calculated FoS at the depth level of PZC/P18 sensor (25.75 mbsf) as a function of slope angle, excess pore pressure, and horizontal acceleration. The three-case calculations (cal 1: $\Delta u = 64$ kPa, cal 2: $\Delta u = 40$ kPa, and cal 3: $\Delta u = 44$ kPa) shown in Figure 12 are considered for three slope angles (10°, 15°, and 20°). For cal 3, we considered four different accelerations (0.001, 0.01, 0.02, and 0.04 g).

temperature trends (Figure 12). PZC/P18 is measuring the pressure within the shear zone at the prone-to-failure area (Figure 3). Unfortunately, we cannot reliably assess to what extent the earthquake caused the observed pore pressure perturbations and if reactivation or evolution of the shear zone occurred, which may have resulted in shear dilatancy of the sediment and pore pressure reduction, followed by the subsequent increase in P18 pore pressure after 14 November 2018. To gain insight into the relationship between seismicity and pore pressure changes, comparison of longer time series or the installation of strain meters would be required.

5.3. What Is the General Transport Mechanism of Pore Water Pressure?

Figure 9 shows the calculation results used to check the working hypothesis that the confined aquifer feeds sedimentary layers equivalent in depth to PZC/P18. For the considered hydraulic diffusivity values, the pore pressure fluctuations imposed at $L = 20$ m (equivalent to PZC/P18 pressure) diffuse rapidly through the sedimentary column at site PZA. From the calculation results of Figure 9 and the strong correlation between measured and predicted values for the first 30 months of monitoring (Figure 9b), it is possible to conclude that site PZA and the level at PZC/P18 are connected to the same pore pressure source as already suggested by Stegmann et al. (2011). Data from Oehler et al. (2017) (Figure 1), which document that cores recovered from the 1979 landslide scar were affected by submarine groundwater seepage, suggest that the base of the prone-to-failure area and the 1979 landslide escarpment are both connected to a fresh water aquifer.

5.4. What Are the Main Factors Influencing the Observed Shear Zone?

The shear zone identified by Sultan et al. (2010) was considered as an indicator of local failure raising questions as to its possible development into a slip surface in response to changes in stress level. Leroueil (2001) and Urciuoli et al. (2007) have already demonstrated that failure process is, at first, local with the formation of plastic zones, then general with the propagation of a failure plane.

To determine the contribution of both pore pressure fluctuations and earthquake loading in the development of shear zones in the study area, we conducted three case calculations (Cal 1, Cal 2, and Cal 3 in Figure 12) with the corresponding pore pressure conditions (Cal 1: $\Delta u = 64$ kPa, Cal 2: $\Delta u = 40$ kPa, and Cal 3: $\Delta u = 44$ kPa). The local peak ground acceleration generated by the Monaco earthquake was shown to be equal to 0.001 g (Courboulex et al., 2020). However, this acceleration strongly depends on morphology (Geli et al., 1988), sediment type, and sediment thickness, (Biscontin & Pestana, 2006). This is why we considered three additional horizontal accelerations exceeding the recorded acceleration for Cal 3, ($k_h = 0.01$ g, 0.02 g, and 0.04 g). FoS is calculated for three different slope angles (10°, 15°, and 20°). The drained geotechnical parameters are those used by Seed et al. (1988): $c' = 0$, $\varphi' = 31°$.

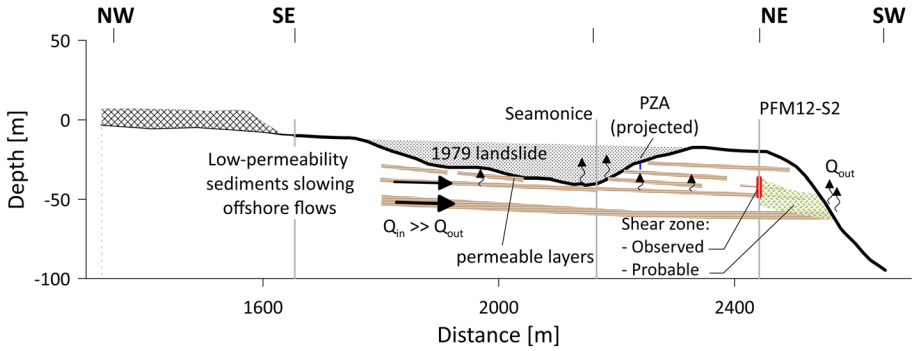

Figure 14. Hydromechanical processes along the profile shown in Figure 1b. The confined aquifer feeds, through low-permeability sediments (Garnier & Gounon, 1984), several permeable layers and is probably the source of the Guglielmi and Prieur (1997) fresh water-springs detected at around 60 m of water depth. One decade of piezometer data confirmed the common source controlling the pore pressure at the base of the prone-to-failure area and the 1979 landslide escarpment. Arrows indicating water flows are projected on the considered cross section so they do not indicate the direction of the main artesian flow direction in the area. Excess pore pressures measured by PZC indicate that inflow from the confined aquifer Q_{in} is much higher than the outflow Q_{out} detected in the water column. PFM12-S2 data show that the shear zone is centered on the excess pore pressure measured by PZC/P18 sensor. An extension of this shear zone is proposed based on Leynaud and Sultan (2010) calculation results indicating that the most probable failure surface is oriented along the NE-SW axis.

For Δu and k_h equal to 0 and total and effective stress increasing linearly with depth (constant submerged unit weight of 7.25 kN/m^3 from Dan et al., 2007), Equation 3 provides a constant FoS with depth (blue curve in Figure 13). Calculated FoS values at the depth level of PZC/P18 sensor (25.75 mbsf) is shown as a function of slope angle, excess pore pressure, and horizontal acceleration (Figure 13). The most critical case corresponds to Cal 3 when k_h is taken as equal to 0.04 g (40 times higher than the acceleration recorded during the local M3.1 earthquake by Courboulex et al., 2020) while the safest case corresponds to Cal 2. Failure (FoS $\leq$ 1) also occurs for Cal 1 when the slope angle is equal to 20° which is very often exceeded at the steep slope of the Var delta front (Figure 1). However, it is important to mention that FoS $\leq$ 1 does not necessarily imply significant displacement; it may cause localized sediment deformation (or shear zone) as the one observed by Sultan et al. (2010) leading to a new equilibrium.

By considering the local acceleration generated by the Monaco earthquake (Courboulex et al., 2020) and the pore pressure measured at PZC/P18, it is obvious that pore pressure is the main factor impacting slope instability and shear zone formation in the area. However, results shown in Figure 13 confirm that minor earthquake shaking could accelerate the progressive slope movement process by decreasing the FoS. On the other hand, the question about the impact of the 3 June 2018 earthquake on the pore pressure measured by PZC/P18 remains unresolved. A reactivation or evolution of the shear zone at PZC may explain this pore pressure perturbation, but we need additional data to be able to conclude on this hypothesis. Future restoration of pressure cyclicity at PZC/P18 would support this supposed coupling between the shear zone, artesian pore pressures, and earthquake shakings.

5.5. Hydromechanical Processes and Implications

Figure 14 illustrates how the previous discussion can be used to characterize the major hydromechanical processes affecting fluid flow fluctuations and the shear zone formation and evolution. Our data suggest that the confined aquifer, having a hydraulic head between 5 and 5.5 m NGF (Ciron et al., 1986), feeds several permeable layers and is probably the source of the fresh water springs detected at around 60 m of water depth (Guglielmi & Prieur, 1997). It is important to mention that despite the large number of acquired in situ geotechnical data and sedimentary cores, the exact geometry and depth of the permeable layers shown in Figure 14 are not yet well constrained. However, one decade of piezometer data acquired from several sites in the scar of the 1979 landslide and in the prone-to-failure area show that diffusion is predominantly responsible for the measured near-seabed pore pressure buildup.

Moreover, our data confirmed what was suspected by Stegmann et al. (2011) about a common source controlling the pore pressure at the base of the prone-to-failure area and the 1979 landslide escarpment. The

amplitude of the measured excess pore pressure is mainly the result of a disequilibrium between fresh water inflow from the confined aquifer (Q_{in}) and outflow in the water column (Q_{out}). The measured high excess pore pressure within the shear zone and the slope stability calculation pointed-out the major role of lateral artesian flow in the slope instability development. Figure 14 shows the possible extension of the shear zone based on Leynaud and Sultan (2010) calculation results indicating that the most probable failure surface is oriented along the NE-SW axis. Despite the slope stability calculations shown in Figure 13, which suggest that earthquake shaking may contribute to shear zone development by decreasing the FoS, it is today premature to conclude about the role of the Monaco 2018 earthquake on the pore pressure perturbations shown in Figure 12.

6. Conclusions

One decade of pore pressure and temperature monitoring, using midterm and long-term piezometer tools, provides data suggesting a groundwater exchange between a coastal confined aquifer and a nearshore shallow-water submarine shelf. Pore pressure fluctuations measured in the scar of the 1979 landslide and in a shear zone at the base of a suspected prone-to-failure area were shown to be connected to a common artesian pressure source. However, those pore water fluctuations are impacted by long, smooth seasonal changes and they did neither synchronize to the discharge of the nearby Var River nor to precipitation in the Nice area, two major sources supplying alluvial aquifers. The presence of low-permeability silt and clay offshore deposits slows down the offshore transmission of groundwater head fluctuations. The slow groundwater lateral flow does not affect the thermal regime and it was established that the seabed temperature and vertical thermal diffusion are the main factors controlling the observed temperature fluctuations.

Although the overpressure measured offshore are sourced from a confined aquifer directly impacted by the discharge of the Var River, the modulation in groundwater head makes it impossible to use available onshore piezometric level data to assess the integrity of the nearshore submarine slope. Those results highlight the advantage, for the present study site, to monitor in situ pore pressure in offshore sedimentary deposits.

Simplified slope stability analyses carried out under drained conditions indicate that pore pressure fluctuation is the main factor impacting slope instability and shear zone formation in the area. Excess pore pressures equivalent to the offshore measured values at 25.75 mbsf are able to bring steep slopes exceeding 20° to failure. We argue that this excess pressure is the major trigger of the detected shear zones at the border of the shelf, off the Nice airport. However, secondary external factors such as earthquake shaking could accelerate the development of progressive failure by decreasing the factor of safety of the slope against failure.

Data Availability Statement

Piezometer data can be downloaded using the following link (http://www.emso-fr.org/EMSO-Ligure-Nice/Data-download).

Acknowledgments

We are grateful to the captains and crews of the R/V *L'Europe* and R/V *Pourquoi Pas*?, for their assistance at sea during four different cruises including STEP 2011 (doi.org:10.17600/11060140), STEP 2014 (doi.org:10.17600/14005400), STEP 2015 (doi.org: 10.17600/15006100), and ESSPENF50_2015 (doi.org 10.17600/15010900). Special thanks to Ronan Apprioual, Mickael Roudaut, and Pierre Guyavarch from Ifremer for ensuring that deployment of piezometers was technically possible. This work benefited from the support of the EU project EMSO (http://www.emso-eu.org/) and of the MODAL project (ANR-17-CE01–0017; http://modal-project.cnrs.fr/) supported by Agence Nationale de la Recherche (ANR) and Deutsche Forschungsgemeinschaft (DFG, Grant KO 2108/26–1) in the framework of a Franco-German research program. The authors thank Adam M. Booth, Associate Editor, and Christian Berndt, Derek Sawyer, and Morelia Urlaub for their comments and constructive reviews. English language editing by Alison Chalm is gratefully acknowledged.

References

Anthony, E. J., & Julian, M. (1997). The 1979 Var Delta landslide on the French Riviera: A retrospective analysis. *Journal of Coastal Research*, *13*(1), 27–35. https://www.jstor.org/stable/4298587

Anthony, E. J., & Julian, M. (1999). Source-to-sink sediment transfers, environmental engineering and hazard mitigation in the steep Var River catchment, French Riviera, southeastern France. *Geomorphology*, *31*(1–4), 337–354. https://doi.org/10.1016/S0169-555X(99)00088-4

Augliera, P., Bethoux, N., Deverchere, J., & Eva, C. (1994). The Ligurian Sea: New seismotectonic evidence. *Bollettino di Geofisica Teorica ed Applicata*, *36*(141–44), 363–380.

Biscontin, G., & Pestana, J. M. (2006). Factors affecting seismic response of submarine slopes. *Natural Hazards and Earth System Sciences*, *6*(1), 97–107. https://doi.org/10.5194/nhess-6-97-2006

Bompais, X., Garziglia, S., Blandin, J., & Hello, Y. (2019). *EMSO-Ligure Nice, a coastal cabled observatory dedicated to the study of slope stability* (pp. 1–8). Marseille, France: OCEANS 2019 - Marseille.

Bromhead, E. N. (1998) *Panel report: Lessons from the Selborne slope stability experiment* (pp. 1589–1592). Rotterdam, The Netherlands: Paper presented at the 2nd International Symposium on Hard Soils—Soft Rocks, Naples, Italy, A. A. Balkema.

Cavalie, O., Sladen, A., & Kelner, M. (2015). Detailed quantification of delta subsidence, compaction and interaction with man-made structures: The case of the NCA airport, France. *Natural Hazards and Earth System Sciences*, *15*(9), 1973–1984. https://doi.org/10.5194/nhess-15-1973-2015

Christophe, L., Scotti, O., & Ioualalen, M. (2012). Reappraisal of the 1887 Ligurian earthquake (western Mediterranean) from macroseismicity, active tectonics and tsunami modelling. *Geophysical Journal International*, *190*(1), 87–104. https://doi.org/10.1111/j.1365-246x.2012.05498.x

Ciron, P., Garnier, J. L., Sedan, O., & Gounon, A. (1986). *Aéroport international de Nice-Côte d'Azur—Extension Sud. Simulation sur modèle mathématique de la décharge de la nappe profonde*, Valbonne, France: BRGM. Retrieved from http://infoterre.brgm.fr/rapports/86-SGN-080-PAC.pdf

Cooper, M. R., Bromhead, E. N., Petley, D. J., & Grant, D. I. (1998). The Selborne cutting stability experiment. *Geotechnique*, *48*(1), 83–101. https://doi.org/10.1680/geot.1998.48.1.83

Courboulex, F., Mercerat, E. D., Deschamps, A., Migeon, S., Baques, M., Larroque, C., et al. (2020). Strong site effect revealed by a new broadband seismometer on the continental shelf offshore Nice airport (southeastern France). *Pure and Applied Geophysics*, *177*(7), 3205–3224. https://doi.org/10.1007/s00024-019-02408-9

Dan, G., Sultan, N., & Savoye, B. (2007). The 1979 Nice harbour catastrophe revisited: Trigger mechanism inferred from geotechnical measurements and numerical modelling. *Marine Geology*, *245*(1–4), 40–64. https://doi.org/10.1016/j.margeo.2007.06.011

de Lange, G. J., Mascle, J., Sakellariou, D., Salamon, A., Rosen, D., Panyides, I., et al. (2011). Marine geohazards in the Mediterranean: Executive summary. In *CIESM Workshop Monographs* (pp. 7–20). Monaco: CIESM.

Du, M. (2016). *Modélisation intégrée des écoulements souterrains et des échanges nappe-rivière dans la basse vallée du Var* (Doctoral dissertation). Côte d'Azur.

Du, M., Fouché, O., Zavattero, E., Ma, Q., Delestre, O., & Gourbesville, P. (2019). Water planning in a mixed land use Mediterranean area: Point-source abstraction and pollution scenarios by a numerical model of varying stream-aquifer regime. *Environmental Science and Pollution Research*, *26*(3), 2145–2166. https://doi.org/10.1007/s11356-018-1437-0

Du, M., Zavattero, E., Ma, Q., Delestre, O., Gourbesville, P., & Fouché, O. (2016). 3D hydraulic modeling of a complex alluvial aquifer for groundwater resource management. *Procedia engineering*, *154*, 340–347. https://doi.org/10.1016/j.proeng.2016.07.487

Dubar, M., & Anthony, E. J. (1995). Holocene environmental change and river-mouth sedimentation in the Baie des Anges, French Riviera. *Quaternary Research*, *43*(3), 329–343. https://doi.org/10.1006/qres.1995.1039

Emily, A., Tennevin, G., & Mangan, C. (2010). *Etude hydrogéologique des nappes profondes de la Basse Vallée du Var*. Nice: Conseil Général Alpes Maritimes.

Eva, E., Solarino, S., & Spallarossa, D. (2001). Seismicity and crustal structure beneath the western Ligurian Sea derived from local earthquake tomography. *Tectonophysics*, *339*(3–4), 495–510. https://doi.org/10.1016/s0040-1951(01)00106-8

Garnier, J. L., & Gounon, A. (1984). *Aéropfe-Côte d'Azur—Extension Sud. Contrôle hydrodynamique de la nappe profonde*. Valbonne, France: BRGM. Retrieved from http://infoterre.brgm.fr/rapports/84-AGI-360-PAC.pdf

Garziglia, S., Sultan, N., Bompais, X., Woerther, P., Roudaut, M., & Apprioual, R. (2019). In *Characterization of the presence of free gas in sediment from long term pore pressure monitoring*, *Geophysical Research Abstracts* (Vol. 21). Vienna: Copernicus.

Garziglia, S., Woerther, P., Apprioual, R., Roudaut, M., Bompais, X., & Barbot, S. (2018). *Pore pressure and temperature data from piezometer SPF-PZ3L-01C on EMSO-LIGURE NICE observatory, since September 2016*, Brest: SEANOE. https://doi.org/10.17882/51528

Geli, L., Bard, P.-Y., & Jullien, B. (1988). The effect of topography on earthquake ground motion: A review and new results. *Bulletin of the Seismological Society of America*, *78*(1), 42–63.

Guglielmi, Y., & Prieur, L. (1997). Locating and estimating submarine freshwater discharge from an interstitial confined coastal aquifer by measurements at sea: Example from the lower Var valley, France. *Journal of Hydrology*, *190*(1–2), 111–122. https://doi.org/10.1016/S0022-1694(96)03061-2

Habib, P. (1994). Aspects géotechniques de l'accident du nouveau port de Nice. *Revue Française de Géotechnique*, *66*, 3–15. https://doi.org/10.1051/geotech/1994066003

Hadj-Hamou, T., & Kavazanjian, E. Jr. (1985). Seismic stability of gentle infinite slopes. *Journal of Geotechnical Engineering*, *111*(6), 681–697. https://doi.org/10.1061/(ASCE)0733-9410(1985)111:6(681)

Ioualalen, M., Migeon, S., & Sardoux, O. (2010). Landslide tsunami vulnerability in the Ligurian Sea: Case study of the 1979 October 16 Nice International Airport submarine landslide and of identified geological mass failures. *Geophysical Journal International*, *181*(2), 724–740. https://doi.org/10.1111/j.1365-246x.2010.04572.x

Kelner, M., Migeon, S., Tric, E., Couboulex, F., Dano, A., Lebourg, T., & Taboada, A. (2014). Recent morphological changes of the Nice continental slope. In *Engineering geology for society and territory* (Vol. 4, pp. 221–225). Cham, Switzerland: Springer.

Kelner, M., Migeon, S., Tric, E., Couboulex, F., Dano, A., Lebourg, T., & Taboada, A. (2016). Frequency and triggering of small-scale submarine landslides on decadal timescales: Analysis of 4D bathymetric data from the continental slope offshore Nice (France). *Marine Geology*, *379*, 281–297. https://doi.org/10.1016/j.margeo.2016.06.009

Klaucke, I., & Cochonat, P. (1999). Analysis of past seafloor failures on the continental slope off Nice (SE France). *Geo-Marine Letters*, *19*(4), 245–253. https://doi.org/10.1007/s003670050115

Kopf, A. J., Kasten, S., & Blees, J. (2010). Geochemical evidence for groundwater-charging of slope sediments: The Nice airport 1979 landslide and tsunami. In D. C. Mosher, R. C. Shipp, L. Moscardelli, J. D. Chaytor, C. D. P. Baxter, H. J. Lee, & R. Urgeles (Eds.), *Submarine mass movements and their consequences* (pp. 203–214). New York: Springer. https://doi.org/10.1007/978-90-481-3071-9_17

Kopf, A. J., Stegmann, S., Garziglia, S., Henry, P., Dennielou, B., Haas, S., & Weber, K.-C. (2016). Soft sediment deformation in the shallow submarine slope off Nice (France) as a result of a variably charged Pliocene aquifer and mass wasting processes. *Sedimentary Geology*, *344*, 290–309. https://doi.org/10.1016/j.sedgeo.2016.05.014

Leroueil, S. (2001). Natural slopes and cuts: Movement and failure mechanisms. *Geotechnique*, *51*(3), 197–243. https://doi.org/10.1680/geot.2001.51.3.197

Leynaud, D., & Sultan, N. (2010). 3-D slope stability analysis: A probability approach applied to the nice slope (SE France). *Marine Geology*, *269*(3–4), 89–106. https://doi.org/10.1016/j.margeo.2009.12.002

Meunier, J., Sultan, N., Jegou, P., & Harmegnies, F. (2004). In *First tests of Penfeld: A new seabed penetrometer* (1–8). Toulon, France: 14th International Offshore and Polar Engineering Conference (ISOPE 2004), International Society of Offshore and Polar Engineers.

Migeon, S., Cattaneo, A., Hassoun, V., Dano, A., Casedevant, A., & Ruellan, E. (2012). Failure processes and gravity-flow transformation revealed by high-resolution AUV swath bathymetry on the Nice continental slope (Ligurian Sea). In *Submarine mass movements and their consequences* (pp. 451–461). Dordrecht, The Netherlands: Springer.

Migeon, S., Cattaneo, A., Hassoun, V., Larroque, C., Corradi, N., Fanucci, F., et al. (2011). Morphology, distribution and origin of recent submarine landslides of the Ligurian margin (North-Western Mediterranean): Some insights into geohazard assessment. *Marine Geophysical Research*, *32*(1–2), 225–243. https://doi.org/10.1007/s11001-011-9123-3

Mulder, T., Migeon, S., Savoye, B., & Faugeres, J. C. (2001). Inversely graded turbidite sequences in the deep Mediterranean: A record of deposits from flood-generated turbidity currents? *Geo-Marine Letters*, *21*(2), 86–93. https://doi.org/10.1007/s003670100071

Mulder, T., Savoye, B., & Syvitski, J. P. M. (1997). Numerical modelling of a mid-sized gravity flow: The 1979 Nice turbidity current (dynamics, processes, sediment budget and seafloor impact) (vol 44, pg 305, 1997). *Sedimentology*, *44*(6), 305–326. https://doi.org/10.1111/j.1365-3091.1997.tb01526.x

Oehler, T., Mogollón, J. M., Moosdorf, N., Winkler, A., Kopf, A., & Pichler, T. (2017). Submarine groundwater discharge within a landslide scar at the French Mediterranean coast. *Estuarine, Coastal and Shelf Science*, *198*, 128–137. https://doi.org/10.1016/j.ecss.2017.09.006

Pégaz-Blanc, O., & Pérot, Y. (2002). *La communauté d'agglomération de Nice Côte d'Azur: Un fort potentiel humain dans un espace à organiser*, Alpes-Côte d'Azur: Insee Provence. Retrieved from http://www.epsilon.insee.fr/jspui/bitstream/1/1594/1/sie48.pdf

Piper, D. J. W., & Savoye, B. (1993). Processes of late Quaternary turbidity current flow and deposition on the Var deep-sea fan, north-west Mediterranean Sea. *Sedimentology*, *40*(3), 557–582. https://doi.org/10.1111/j.1365-3091.1993.tb01350.x

Roesner, A., Wiemer, G., Kreiter, S., Wenau, S., Wu, T.-W., Courboulex, F., et al. (2019). Impact of seismicity on Nice slope stabilityLigurian basin, SE France: A geotechnical revisit. *Landslides*, *16*(1), 23–35. https://doi.org/10.1007/s10346-018-1060-7

Rohmer, O., Bertrand, E., Mercerat, E. D., Régnier, J., Pernoud, M., Langlaude, P., & Alvarez, M. (2020). Combining borehole log-stratigraphies and ambient vibration data to build a 3D model of the lower Var Valley, Nice (France). *Engineering Geology*, *270*, 105588. https://doi.org/10.1016/j.enggeo.2020.105588

Savoye, B., Piper, D. J. W., & Droz, L. (1993). Plio-Pleistocene evolution of the Var deep-sea fan off the French Riviera. *Marine and Petroleum Geology*, *10*(6), 550–571. https://doi.org/10.1016/0264-8172(93)90059-2

Seed, H. B., Seed, R. B., Schlosser, F., Blondeau, F., & Juran, I. (1988). *The landslide at the port of Nice on October 16, 1979 (Rep. No. UCB/EERC-88, 10)*, California: University of California.

Stegmann, S., Sultan, N., Kopf, A., Apprioual, R., & Pelleau, P. (2011). Hydrogeology and its effect on slope stability along the coastal aquifer of Nice, France. *Marine Geology*, *280*(1–4), 168–181. https://doi.org/10.1016/j.margeo.2010.12.009

Sultan, N., & Lafuerza, S. (2013). In situ equilibrium pore-water pressures derived from partial piezoprobe dissipation tests in marine sediments. *Canadian Geotechnical Journal*, *50*(12), 1294–1305. https://doi.org/10.1139/cgj-2013-0062

Sultan, N., Savoye, B., Jouet, G., Leynaud, D., Cochonat, P., Henry, P., et al. (2010). Investigation of a possible submarine landslide at the Var delta front (Nice continental slope, Southeast France). *Canadian Geotechnical Journal*, *47*(4), 486–496. https://doi.org/10.1139/t09-105

Urciuoli, G., Picarelli, L., & Leroueil, S. (2007). Local soil failure before general slope failure. *Geotechnical and Geological Engineering*, *25*(1), 103–122. https://doi.org/10.1007/s10706-006-0009-0